

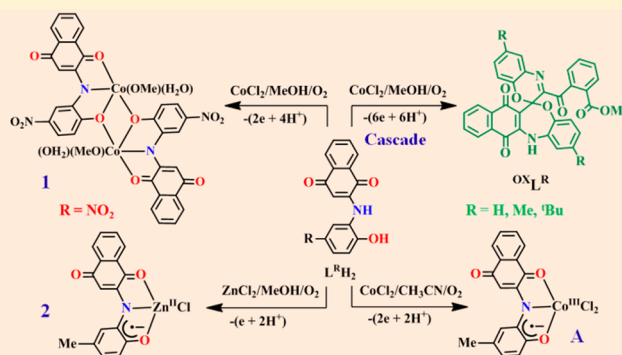
# Cobalt Ion Promoted Redox Cascade: A Route to Spiro Oxazine-Oxazepine Derivatives and a Dinuclear Cobalt(III) Complex of an *N*-(1,4-Naphthoquinone)-*o*-aminophenol Derivative

Sandip Mondal, Sachinath Bera, Suvendu Maity, and Prasanta Ghosh\*<sup>ID</sup>

Department of Chemistry, R. K. Mission Residential College, Narendrapur, Kolkata 103, West Bengal, India

## Supporting Information

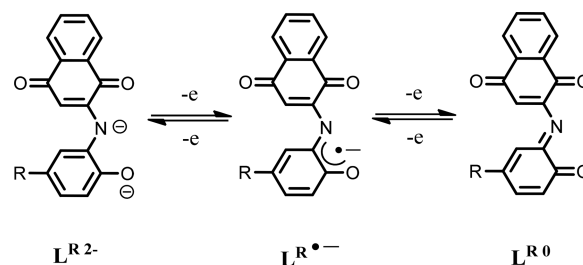
**ABSTRACT:** The study discloses that the redox activity of *N*-(1,4-naphthoquinone)-*o*-aminophenol derivatives ( $L^R H_2$ ) containing a (phenol)-NH-(1,4-naphthoquinone) fragment is notably different from that of a (phenol)-NH-(phenol) precursor. The former is a platform for a redox cascade.  $L^R H_2$  is redox noninnocent and exists in Cat-N-(1,4-naphthoquinone)(2<sup>-</sup>) ( $L^{R 2-}$ ) and SQ-N-(1,4-naphthoquinone) ( $L^{R \bullet -}$ ) states in the complexes. Reactions of  $L^R H_2$  with cobalt(II) salts in MeOH in air promote a cascade affording spiro oxazine-oxazepine derivatives ( $OX_L^R$ ) in good yields, when R = H, Me, <sup>t</sup>Bu. Spiro oxazine-oxazepine derivatives are bioactive, and such a molecule has so far not been isolated by a schematic route. In this context this cascade is significant. Dimerization of  $L^R H_2 \rightarrow OX_L^R$  in MeOH is a (6H<sup>+</sup> + 6e) oxidation reaction and is composed of formations of four covalent bonds and 6-exo-trig and 7-endo-trig cyclization based on C–O coupling reactions, where MeOH is the source of a proton and the ester function. It was established that the active cascade precursor is [ $L^{Me \bullet -}$ Co<sup>III</sup>Cl<sub>2</sub>] (A). Notably, formation of a spiro derivative was not detected in CH<sub>3</sub>CN and the reaction ends up furnishing A. The route of the reaction is tunable by R, when R = NO<sub>2</sub>, it is a (2e + 4H<sup>+</sup>) oxidation reaction affording a dinuclear  $L^{R 2-}$  complex of cobalt(III) of the type [ $(L^{NO_2 2-})_2 Co^{III}_2(OMe)_2(H_2O)_2$ ] (1) in good yields. No cascade occurs with zinc(II) ion even in MeOH and produces a  $L^{Me \bullet -}$  complex of type [ $(L^{Me \bullet -})Zn^{II}Cl_2$ ] (2). The intermediate A and 2 exhibit strong EPR signals at *g* = 2.008 and 1.999, confirming the existence of  $L^{Me \bullet -}$  coordinated to low-spin cobalt(III) and zinc(II) ions. The intermediates of  $L^R H_2 \rightarrow OX_L^R$  conversion were analyzed by ESI mass spectrometry. The molecular geometries of  $OX_L^R$  and 1 were confirmed by X-ray crystallography, and the spectral features were elucidated by TD DFT calculations.



## INTRODUCTION

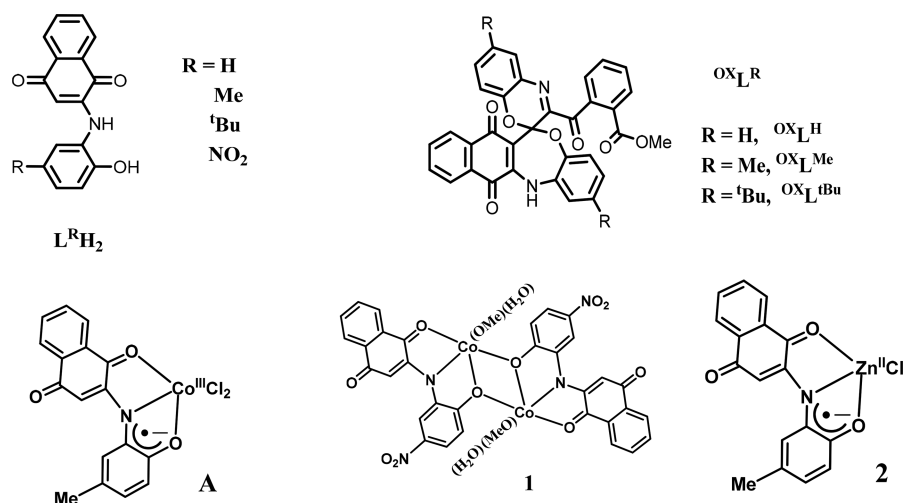
The redox activity of bis(3,5-di-*tert*-butyl-2-phenyl)amine ( $L^{ONO}H_3$ ), a ONO donor ligand that contains a (phenol)-NH-(phenol) fragment, is versatile and significant in chemical science. Transition-metal complexes of  $L^{ONO}H_3$  are worthy in the context of electronic structure, catalytic activity, valence tautomerism, and spin-crossover phenomena.<sup>1–3</sup> Numerous Co<sup>II</sup>/Co<sup>III</sup> complexes of  $L^{ONO}H_3$  having Cat-N-BQ(1<sup>-</sup>) and Cat-N-SQ(2<sup>-</sup>) electronic states that exhibit valence tautomerism were reported.<sup>4,5</sup> In this regard, the coordination chemistry of a molecule that contains a (phenol)-NH-(quinone) fragment and its functionality have been the subjects of investigation. The same was explored in this project, and it was authenticated that the reactivities of the two types of fragments are remarkably different. In this investigation the chemistry of *N*-(1,4-naphthoquinone)-*o*-aminophenol derivatives ( $L^R H_2$ ) having a phenol-NH-(1,4-naphthoquinone) fragment which exists as Cat-N-(1,4-naphthoquinone)(2<sup>-</sup>) ( $L^{R 2-}$ ), SQ-N-(1,4-naphthoquinone) ( $L^{R \bullet -}$ ), and Q-N-(1,4-naphthoquinone) ( $L^{R 0}$ ) states as depicted in Scheme 1 is disclosed.

Scheme 1. Redox States of  $L^R H_2$  Ligands



It was established that the reaction of  $L^R H_2$  with cobalt(II) salts in MeOH promotes a redox cascade generating spiro oxazine-oxazepine derivatives, methyl 2-(2',6-bis(R)-7',12'-dioxo-12',13'-dihydro-7'*H*-spiro[benzo[*b*][1,4]oxazine-2,6'-benzo[*b*]naphtho[2,3-*e*][1,4]oxazepin]-3-ylcarbonyl)benzoate ( $OX_{LR}$ ), as shown in Chart 1, when R = H, Me, <sup>t</sup>Bu and the

Received: August 1, 2017

Chart 1. Isolated  $\text{OxL}^{\text{R}}$  Derivatives and Metal Complexes

cascade precursor is  $[(\text{L}^{\text{Me}})^{\bullet-}\text{Co}^{\text{III}}\text{Cl}_2]$  (A), which was successfully isolated from the same reaction in  $\text{CH}_3\text{CN}$ .

Finding a cascade route to isolate a bioactive organic molecule is a challenge in chemical science and pharmacy.<sup>6</sup> Cascades are significant in reducing chemical waste and increasing atom economy.<sup>7</sup> Various types of cascades have been established to develop the syntheses of functional organic molecules.<sup>8,9</sup> However, a cascade that is composed of multistep redox reactions is rare.<sup>10</sup> Recently a metal ion promoted redox cascade converting *N*-(1,4-dioxo-1,4-dihydronaphthalen-2-yl)-benzohydrazide ( $\text{LH}_2$ ) to a stable zwitterionic triphenylphosphonio-hydrazyl radical ( $^{\text{PPH}_3}\text{L}^{\bullet\pm}$ ) and a hitherto unknown diarylindazolo[3a,3c]indazole ( $^{\text{Ind}}\text{L}_2$ ) derivative were reported.<sup>11</sup> In this particular project a redox cascade that yields bioactive spiro oxazine-oxazepine derivatives containing a *p*-quinone fragment was authenticated. The multicomponent cascade, which involves metal coordination, C–C coupling, tautomerization, oxidation, nucleophilic addition of alcohol, ring cleavage, and 6-*exo*-trig and 7-*endo*-trig C–O coupling reactions converting  $\text{L}^{\text{R}}\text{H}_2$  to  $\text{OxL}^{\text{R}}$  reported in this article, is overall a  $(6e + 6\text{H}^+)$  oxidation reaction.

The wide range of biological activities of oxazine<sup>12</sup> and oxazepine<sup>13</sup> heterocycles imply that a molecule having both oxazine and oxazepine fragments will be more promising in exploring pharmaceutical activities. The numerous other functionalities of the oxazine and oxazepine derivatives make these heterocycles precious in chemical science.<sup>14</sup> However, no substantive report on a spiro oxazine-oxazepine derivative is available so far. In this context the report is relevant and worthy.

One of the significant observations is that the route of the reaction can be tuned by changing R. It was established that, when  $\text{R} = \text{NO}_2$ ,  $\text{L}^{\text{R}2-}$  acts as a tridentate dianionic ONO donor ligand and no 1,4-addition and C–O coupling reactions generating  $\text{OxL}^{\text{NO}_2}$  were substantiated. Rather, the reaction affords a dinuclear cobalt(III) Cat-N-(1,4-naphthoquinone) ( $2-$ ) complex of the type  $[(\text{L}^{\text{NO}_2 2-})_2\text{Co}^{\text{III}}_2(\text{OMe})_2(\text{H}_2\text{O})_2]$  (1). Because of the nitro group, the Cat-N-(1,4-naphthoquinone) chelate is stabilized in 1. The reaction path depends also on the solvent and metal ion used. In  $\text{CH}_3\text{CN}$ , no cascade progresses. No cascade was established using zinc(II) ion even in MeOH solvent; rather the reaction affords a  $\text{L}^{\text{Me}\bullet-}$  complex of zinc(II) of the type  $[(\text{L}^{\text{Me}\bullet-})\text{Zn}^{\text{II}}\text{Cl}_2]$  (2) in good yields. The

mechanistic aspects of  $\text{L}^{\text{R}}\text{H}_2 \rightarrow \text{OxL}^{\text{R}}$  conversions have been critically analyzed by ESI mass spectrometry. The molecular geometries of  $\text{OxL}^{\text{R}}$  and 1 were successfully authenticated by single-crystal X-ray crystallography.

## EXPERIMENTAL SECTION

**Materials and Physical Measurements.** Reagents or analytical grade materials were obtained from commercial suppliers and used without further purification. Spectroscopic grade solvents were used for spectroscopic and electrochemical measurements. The C, H, and N contents of the compounds were obtained from a PerkinElmer 2400 Series II elemental analyzer. Infrared spectra of the samples were measured from 4000 to  $400\text{ cm}^{-1}$  with KBr pellets at room temperature on a PerkinElmer Spectrum RX 1 FT-IR spectrophotometer.  $^1\text{H}$  and  $^{13}\text{C}$  NMR spectra in  $\text{CDCl}_3$  solvent were recorded at 296 K on a Bruker Avance 500/300 MHz spectrometer. ESI mass spectra were recorded on a Shimadzu LCMS 2020 mass spectrometer equipped with an electrospray ionization (ESI) ion source. Electronic absorption spectra in solution were obtained on a PerkinElmer Lambda 750 spectrophotometer in the range 3300–175 nm. The electroanalytical instrument BASi Epsilon-EC for cyclic voltammetry experiments in  $\text{CH}_2\text{Cl}_2$  solutions containing 0.2 M tetrabutylammonium hexafluorophosphate as supporting electrolyte was used. A BASi platinum working electrode, platinum auxiliary electrode, and Ag/AgCl reference electrode were used for the measurements. The redox potential data are referenced vs the ferrocenium/ferrocene ( $\text{Fc}^+/\text{Fc}$ ) couple.

**Syntheses.** *2-((2-Hydroxyphenyl)amino)naphthalene-1,4-dione* ( $\text{L}^{\text{H}}\text{H}_2$ ). To a solution of 1,4-naphthoquinone (1.58 g, 10 mmol) in MeOH was added 2-aminophenol (1.1 g, 10 mmol), and the resulting mixture was stirred for 24 h at room temperature in air. A red solid separated out, which was filtered and dried in air. Yield: 2.10 g (75%). Anal. Calcd for  $\text{C}_{16}\text{H}_{11}\text{NO}_3$ : C, 72.45; H, 4.18; N, 5.28. Found: C, 72.02; H, 4.09; N, 5.20. Mass spectrum (ESI):  $m/z$  264 for  $[\text{L}^{\text{H}}\text{H}_2]^-$ .  $^1\text{H}$  NMR (300 MHz,  $\text{CDCl}_3$ ):  $\delta$  (ppm) 9.02 (s, 1H), 8.57 (s, 1H), 7.83–7.78 (m, 2H), 7.71 (d,  $J = 7.8$  Hz, 1H), 7.44 (t,  $J = 7.5$  Hz, 1H), 7.3 (t,  $J = 7.8$  Hz, 1H), 7.20 (d,  $J = 7.2$  Hz, 1H), 7.00 (t,  $J = 6.9$  Hz, 1H), 6.94 (d,  $J = 6.8$  Hz, 1H), 6.86 (t,  $J = 7.8$  Hz, 1H). IR/ $\text{cm}^{-1}$  (KBr):  $\nu$  3439 (s, –OH), 3281 (s, NH), 1682 (s, CO), 1598 (s), 1553 (s), 1459 (s), 1274 (s), 1104 (m), 990 (m), 740 (m).

*2-((2-Hydroxy-5-methylphenyl)amino)naphthalene-1,4-dione* ( $\text{L}^{\text{Me}}\text{H}_2$ ). To a solution of 1,4-naphthoquinone (1.58 g, 10 mmol) in MeOH was added 2-amino-4-methylphenol (1.1 g, 10 mmol), and the resulting mixture was stirred for 24 h at room temperature in air. A red solid separated out, which was filtered and dried in air. Yield: 1.5 g (54%). Anal. Calcd for  $\text{C}_{17}\text{H}_{13}\text{NO}_3$ : C, 73.37; H, 4.35; N, 5.03. Found: C, 73.03; H, 4.28; N, 4.92. Mass spectrum (ESI):  $m/z$  277 for

Table 1. X-ray Crystallographic Data of  $\text{OxL}^{\text{Me}}$ ,  $\text{OxL}^{\text{tBu}}$ , and **1**

	$\text{OxL}^{\text{Me}}$	$\text{OxL}^{\text{tBu}}$	<b>1</b>
formula	$\text{C}_{35}\text{H}_{24}\text{N}_2\text{O}_7$	$\text{C}_{41}\text{H}_{33}\text{N}_2\text{O}_7$	$\text{C}_{34}\text{H}_{28}\text{Co}_2\text{N}_4\text{O}_{14}$
CCDC no.	1561962	1561963	1561964
fw	584.56	665.62	834.43
cryst color	red	red	black
cryst syst	monoclinic	triclinic	monoclinic
space group	$P2_1/c$	$P\bar{1}$	$P2_1/n$
<i>a</i> (Å)	8.3860(5)	10.6902(4)	7.5672(2)
<i>b</i> (Å)	17.4124(11)	11.6467(4)	22.3208(6)
<i>c</i> (Å)	18.5375(12)	15.6382(6)	10.0679(3)
$\beta$ (deg)	90	109.546(2)	101.129(1)
<i>V</i> (Å <sup>3</sup> )	2706.9(3)	1698.55(11)	1668.55(8)
<i>Z</i>	4	2	2
<i>T</i> (K)	293(2)	293(2)	293(2)
no. of rflns collected ( $2\theta_{\text{max}}$ )	27529/50.14	23925/51.46	19099/52.78
$\rho_{\text{calcd}}$ (g cm <sup>-3</sup> )	1.434	1.308	1.653
no. of unique rflns/rflns with $I > 2\sigma$	4766/4317	6429/3924	3419/2812
$\mu$ (mm <sup>-1</sup> )/ $\lambda$ (Å)	0.101/0.71073	0.090/0.71073	1.074/0.71073
<i>F</i> (000)	1216.0	704.0	844
$R1^b$ /goodness of fit <sup>c</sup>	0.0950/1.189	0.0581/0.978	0.0407/1.140
$wR2^d$ ( $I > 2\sigma(I)$ )	0.3047	0.1455	0.1051
no. of params/restraints	400/0	466/0	254
residual density (e Å <sup>-3</sup> )	0.454/−0.458	0.312/−0.282	0.702/−0.365

<sup>a</sup>Observation criterion:  $I > 2\sigma(I)$ . <sup>b</sup> $R1 = \sum ||F_o| - |F_c|| / \sum |F_o|$ . <sup>c</sup>GOF =  $\{\sum [w(F_o^2 - F_c^2)] / (n - p)\}^{1/2}$ . <sup>d</sup> $wR2 = \{\sum [w(F_o^2 - F_c^2)^2] / \sum [w(F_o^2)^2]\}^{1/2}$ , where  $w = 1/[\sigma^2(F_o^2) + (aP)^2 + bP]$  and  $P = (F_o^2 + 2F_c^2)/3$ .

$[\text{L}^{\text{Me}}\text{H}_2]^-$ . <sup>1</sup>H NMR (300 MHz, CDCl<sub>3</sub>):  $\delta$  (ppm) 8.01 (broad, 2H), 7.76–7.55 (m, 4H), 7.15 (s, 1H), 6.78 (t,  $J = 7.5$  Hz, 2H), 6.34 (s, 1H), 2.29 (s, 3H). IR/cm<sup>-1</sup> (KBr):  $\nu$  3437 (s, OH), 3319 (s, NH), 2924 (m), 1682 (s, CO), 1624 (m), 1599 (s), 1566 (s), 1360 (m), 1300 (m), 1166 (m), 610 (m).

2-((5-(*tert*-Butyl)-2-hydroxyphenyl)amino)naphthalene-1,4-dione ( $\text{L}^{\text{tBu}}\text{H}_2$ ). To a solution of 1,4-naphthoquinone (1.58 g, 10 mmol) in MeOH was added 2-amino-4-(*tert*-butyl)phenol (1.65 g, 10 mmol), and the resulting mixture was stirred for 24 h at room temperature in air. A red solid separated out, which was filtered and dried in air. Yield: 2.4 g (75%). Anal. Calcd for  $\text{C}_{20}\text{H}_{19}\text{NO}$ : C, 74.75; H, 5.96; N, 4.36. Found: C, 74.52; H, 5.87; N, 4.26. Mass spectrum (ESI):  $m/z$  320 for  $[\text{L}^{\text{tBu}}\text{H}_2]^-$ . <sup>1</sup>H NMR (300 MHz, CDCl<sub>3</sub>):  $\delta$  (ppm) 8.09 (broad, 2H), 7.74–7.57 (m, 4H), 7.10 (s, 1H), 6.88 (t,  $J = 7.5$  Hz, 2H), 6.20 (s, 1H), 1.64 (s, 9H). IR/cm<sup>-1</sup> (KBr):  $\nu$  3432 (s, OH), 3350 (s, NH), 1679 (s, CO), 1597 (s), 1500 (m), 1360 (m), 1300 (m), 994 (m), 723 (m).

2-((2-Hydroxy-5-nitrophenyl)amino)naphthalene-1,4-dione ( $\text{L}^{\text{NO}_2}\text{H}_2$ ). To a solution of 1,4-naphthoquinone (1.58 g, 10 mmol) in MeOH was added 2-amino-4-nitrophenol (1.54 g, 10 mmol), and the resulting mixture was stirred for 24 h at room temperature in air. A red solid separated out, which was filtered and dried in air. Yield: 2.22 g (71%). Anal. Calcd for  $\text{C}_{16}\text{H}_{10}\text{N}_2\text{O}_5$ : C, 61.94; H, 3.25; N, 9.03. Found: C, 61.63; H, 3.19; N, 8.94. Mass spectrum (ESI):  $m/z$  309 for  $[\text{L}^{\text{NO}_2}\text{H}_2]^-$ . <sup>1</sup>H NMR (300 MHz, CDCl<sub>3</sub>):  $\delta$  (ppm) 11.6 (s, OH), 8.83 (s, NH), 7.99 (d,  $J = 7.5$  Hz, 1H), 7.95 (t,  $J = 7.2$  Hz, 2H), 7.90 (d,  $J = 7.8$  Hz, 1H), 7.86–7.80 (m, 3H), 7.13 (d,  $J = 8.5$  Hz, 1H). IR/cm<sup>-1</sup> (KBr):  $\nu$  3385 (s, OH), 3300 (s, NH), 1670 (s, CO), 1620 (s), 1565 (s), 1503 (m), 1350 (s), 1128 (m), 1086 (m), 923 (m).

Methyl 2-(7',12'-Dioxo-12',13'-dihydro-7'H-spiro[benzo[b][1,4]oxazine-2,6'-benzo[b]naphtho[2,3-e][1,4]oxazepin]-3-ylcarbonyl)benzoate ( $\text{OxL}^{\text{H}}$ ). To a suspension of  $\text{L}^{\text{Me}}\text{H}_2$  (66 mg, 0.25 mmol) in MeOH (25 mL) in a round-bottom flask were carefully added  $\text{CoCl}_2 \cdot 6\text{H}_2\text{O}$  (60 mg, 0.25 mmol) followed by triethylamine (1 drop, 0.50 mmol) in MeOH (5 mL). The solution turned green and slowly changed to red; it was then allowed to evaporate slowly in air. After 4–5 days, a red crystalline compound of  $\text{OxL}^{\text{H}}$  separated out, which was collected upon filtration and dried in air. Yield: 15 mg (20% with respect to  $\text{L}^{\text{H}}\text{H}_2$ ). The same reaction was performed with  $\text{Co}(\text{NO}_3)_2 \cdot$

$6\text{H}_2\text{O}$ , and the yield was 18 mg (25% with respect to  $\text{L}^{\text{H}}\text{H}_2$ ). Anal. Calcd for  $\text{C}_{33}\text{H}_{20}\text{N}_2\text{O}_7$ : C, 71.22; H, 3.62; N, 5.03. Found: C, 70.98; H, 3.51; N, 4.89. Mass spectrum (ESI):  $m/z$  556 for  $[\text{OxL}^{\text{H}}]^+$ . <sup>1</sup>H NMR (500 MHz, CDCl<sub>3</sub>):  $\delta$  (ppm) 8.41 (s, NH), 8.18 (d,  $J = 10$ , 1H), 8.06 (d,  $J = 10$  Hz, 1H), 7.99 (d,  $J = 9.5$  Hz, 1H), 7.74 (t,  $J = 10$  and 10 Hz, 2H), 7.72 (t,  $J = 10$  and 10 Hz, 1H), 7.61–7.51 (m, 3H), 7.26–7.11 (m, 3H), 6.93–6.91 (m, 2H), 6.61 (d,  $J = 10$ , 1H), 6.38 (d,  $J = 11.5$ , 1H), 3.73 (s, 3H). <sup>13</sup>C NMR (500 MHz, CDCl<sub>3</sub>):  $\delta$  (ppm) 193.1, 181.2, 180.9, 167.6, 154, 144, 143, 140, 139.9, 135.5, 134.1, 133.0, 131.9, 131.7, 131.1, 129.9, 129.3, 128.4, 127, 126.9, 126.7, 126, 125.6, 125.2, 124, 124.5, 123.5, 120.7, 120, 116.6, 116, 52.3, 29.8. IR/cm<sup>-1</sup> (KBr):  $\nu$  3313 (s, NH), 1736 (s, –COOMe), 1677 (s, CO), 1590 (s), 1507 (s), 1443 (m), 1300 (s), 1127 (s), 1084 (s), 760 (m).

Methyl 2-(2',6'-Dimethyl-7',12'-dioxo-12',13'-dihydro-7'H-spiro[benzo[b][1,4]oxazine-2,6'-benzo[b]naphtho[2,3-e][1,4]oxazepin]-3-ylcarbonyl)benzoate ( $\text{OxL}^{\text{Me}}$ ). To a suspension of  $\text{L}^{\text{Me}}\text{H}_2$  (70 mg, 0.25 mmol) in MeOH (25 mL) in a round-bottom flask were added carefully  $\text{CoCl}_2 \cdot 6\text{H}_2\text{O}$  (60 mg, 0.25 mmol) followed by triethylamine (1 drop, 0.50 mmol) in MeOH (5 mL). The solution turned green and slowly changed to red; it was then allowed to evaporate slowly in air. After 4–5 days, red crystals of  $\text{OxL}^{\text{Me}}$  separated out, which were collected upon filtration and dried in air. Yield: 28 mg (41% with respect to  $\text{L}^{\text{Me}}\text{H}_2$ ). The same reaction was performed with  $\text{Co}(\text{NO}_3)_2 \cdot 6\text{H}_2\text{O}$ , and the yield was 31.5 mg (46% with respect to  $\text{L}^{\text{Me}}\text{H}_2$ ). Anal. Calcd for  $\text{C}_{35}\text{H}_{24}\text{N}_2\text{O}_7$ : C, 71.91; H, 4.14; N, 4.79. Found: C, 71.63; H, 4.02; N, 4.68. Mass spectrum (ESI):  $m/z$  584 for  $[\text{OxL}^{\text{Me}}]^+$ . <sup>1</sup>H NMR (300 MHz, CDCl<sub>3</sub>):  $\delta$  (ppm) 8.35 (s, 1H, –NH), 8.17 (d,  $J = 7.5$ , 1H), 8.06 (d,  $J = 7.2$ , 1H), 7.99 (d,  $J = 7.2$ , 1H), 7.78–7.67 (m, 2H), 7.63–7.49 (m, 3H), 7.32 (s, 1H), 7.03 (d,  $J = 7.8$ , Hz, 1H), 6.94 (s, 1H), 6.73 (d,  $J = 8.1$ , 1H), 6.52 (d,  $J = 8.4$ , 1H), 6.28 (d,  $J = 8.1$ , 1H), 3.73 (s, 3H, –OMe), 2.33 (s, 6H). IR/cm<sup>-1</sup> (KBr):  $\nu$  3260 (s, NH), 2985 (m), 1736 (s, –COOMe), 1677 (s, CO), 1590 (s), 1507 (s), 1443 (m), 1300 (s), 1127 (s), 1084 (s), 760 (m).

Methyl 2-(2',6'-Di-*tert*-butyl-7',12'-dioxo-12',13'-dihydro-7'H-spiro[benzo[b][1,4]oxazine-2,6'-benzo[b]naphtho[2,3-e][1,4]oxazepin]-3-ylcarbonyl)benzoate ( $\text{OxL}^{\text{tBu}}$ ). It was prepared by the above procedure from  $\text{L}^{\text{tBu}}\text{H}_2$  using  $\text{CoCl}_2 \cdot 6\text{H}_2\text{O}$  and MeOH as a solvent. Yield: 40 mg (54% with respect to  $\text{L}^{\text{tBu}}\text{H}_2$ ). Yield: 50 mg (68% with respect to  $\text{L}^{\text{tBu}}\text{H}_2$ ) when  $\text{Co}(\text{NO}_3)_2 \cdot 6\text{H}_2\text{O}$  was used. Anal. Calcd

for  $C_{41}H_{36}N_2O_7$ : C, 73.64; H, 5.43; N, 4.19. Found: C, 73.49; H, 5.35; N, 4.09. Mass spectrum (ESI):  $m/z$  668 for  $[(L^{Me})Co^{III}]^+$ .  $^1H$  NMR (300 MHz,  $CDCl_3$ ):  $\delta$  (ppm) 8.38 (s, 1H, -NH), 8.16 (d,  $J = 8.4$  Hz, 1H), 8.04 (d,  $J = 7.2$  Hz, 1H), 7.99 (d,  $J = 7.2$  Hz, 1H), 7.71 (t,  $J = 9.6$  Hz, 2H), 7.60–7.50 (m, 4H), 7.10 (s, 1H), 6.98 (d,  $J = 9.5$  Hz, 1H), 6.95 (d,  $J = 9.5$  Hz, 1H), 6.58 (d,  $J = 8.7$  Hz, 1H), 6.37 (d,  $J = 8.4$  Hz, 1H), 3.73 (s, 3H), 1.32 (s, 9H), 1.25 (s, 9H). IR/ $cm^{-1}$  (KBr):  $\nu$  3255 (s, NH), 2970 (m), 1736 (s, COOMe), 1680 (s, CO), 1612 (s), 1540 (m), 1289 (s), 1134 (m), 983 (m), 720 (m).

$[(L^{Me})Co^{III}Cl_2]$  (A). To a solution of  $L^{Me}H_2$  (70 mg, 0.25 mmol) in  $CH_3CN$  (25 mL) in a 100 mL round-bottom flask were added carefully  $CoCl_2 \cdot 6H_2O$  (60 mg, 0.25 mmol) followed by triethylamine (1 drop, 0.50 mmol). The solution turned green. It was stirred for 2 h and a green precipitate separated out, which was collected upon filtration and dried in air. Yield: 51 mg (50% with respect to cobalt). Anal. Calcd for  $C_{17}H_{11}Cl_2CoNO_3$ : C, 50.15; H, 2.72; N, 3.44. Found: C, 49.98; H, 2.67; N, 3.36. Mass spectrum (ESI):  $m/z$  406 for  $[A]^+$ . IR/ $cm^{-1}$  (KBr):  $\nu$  2935 (m), 1684 (s, CO), 1596 (m), 1514 (s), 1297 (m), 1245 (s), 1110 (m), 819 (m), 720 (s).

$[(L^{NO_2})_2Co^{III}(OMe)_2(H_2O)_2]$  (1). To a solution of  $L^{NO_2}H_2$  (78 mg, 0.25 mmol) in MeOH (25 mL) in a 100 mL round-bottom flask, were added carefully  $CoCl_2 \cdot 6H_2O$  (60 mg, 0.25 mmol) followed by triethylamine (1 drop, 0.50 mmol), and the mixture was stirred. The solution turned green and was allowed to evaporate slowly in air. After 2–3 days, black crystals of **1** separated out, which were collected upon filtration and dried in air. Yield: 41 mg (40% with respect to cobalt). Anal. Calcd for  $C_{34}H_{26}Co_2N_4O_{14}$ : C, 49.06; H, 3.15; N, 6.73. Found: C, 48.92; H, 3.11; N, 6.66. Mass spectrum (ESI):  $m/z$  832 for  $[1]^+$ .  $^1H$  NMR (500 MHz,  $CDCl_3$ ):  $\delta$  (ppm) 8.21 (s, 1H), 7.9 (d, 2H), 7.6 (d, 2H), 6.25 (s, 1H), 5.96 (t, 2H), 3.38 (s, 3H), 2.5 (s, 2H). IR/ $cm^{-1}$  (KBr):  $\nu$  3420 (s,  $H_2O$ ), 2924 (m), 1597 (s), 1516 (s), 1299 (s), 1254 (s), 1119 (m), 812 (m), 712 (m).

$[(L^{Me})Zn^{II}Cl]$  (2). To a suspension of  $L^{Me}H_2$  (70 mg, 0.25 mmol) in MeOH (25 mL) in a 100 mL round-bottom flask were added carefully  $ZnCl_2 \cdot 6H_2O$  (61 mg, 0.50 mmol) followed by triethylamine (1 drop, 0.50 mmol). The solution turned bluish-green and was allowed to evaporate slowly in air. After 2–3 days, a blue mass of **2** separated out, which was collected upon filtration and dried in air. Yield: 71 mg (75% with respect to zinc). Anal. Calcd for  $C_{17}H_{11}ClNO_3Zn$ : C, 54.00; H, 2.93; N, 3.70. Found: C, 53.75; H, 2.87; N, 3.62. Mass spectrum (ESI):  $m/z$  376 for  $[1]^+$ . IR/ $cm^{-1}$  (KBr):  $\nu$  2915 (m), 1650 (m), 1586 (m), 1502 (s), 1450 (m), 1312 (m), 1250 (s), 853 (m), 1254 (s), 766 (m).

**Single-Crystal X-ray Structure Determinations of the Complexes (CCDC 1561962–1561964).** Single crystals of  $OX_L^{Me}$ ,  $OX_L^{tBu}$ , and **1** were picked up with nylon loops and were mounted on a Bruker AXS D8 QUEST ECO diffractometer equipped with a Mo target rotating-anode X-ray source and a graphite monochromator (Mo  $K\alpha$ ,  $\lambda = 0.71073$  Å). Final cell constants were obtained from least-squares fits of all measured reflections. Intensity data were corrected for absorption using intensities of redundant reflections. The structures were readily solved by direct methods and subsequent difference Fourier techniques. The crystallographic data are given in Table 1. The Siemens SHELXS-97 software package was used for solution, and SHELXL-97 was used for the refinement.<sup>15</sup> All non-hydrogen atoms were refined anisotropically. Hydrogen atoms were placed at calculated positions and refined as riding atoms with isotropic displacement parameters.

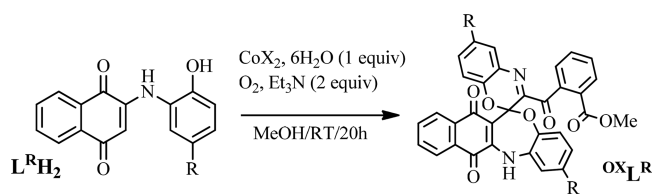
**Density Functional Theory (DFT) Calculations.** All calculations reported in this article were done with the Gaussian 03W<sup>16</sup> program package supported by Gauss View 4.1. The DFT<sup>17</sup> calculations were performed at the level of the Becke three-parameter hybrid functional with the nonlocal correlation functional of Lee–Yang–Parr (B3LYP).<sup>18</sup> The gas-phase geometry of  $[(L^{NO_2})Co^{III}(OMe)(H_2O)]$ , a mononuclear unit of **1** with singlet spin state, was optimized using Pulay's direct inversion<sup>19</sup> in the iterative subspace (DIIS) "tight" convergent SCF procedure,<sup>20</sup> ignoring symmetry. In all calculations, a LANL2DZ basis set along with the corresponding effective core potential was used for cobalt metal.<sup>21</sup> The valence double- $\zeta$  basis set 6-31<sup>22</sup> was used for the H atoms. For C, N, and O atoms, the valence

double- $\zeta$  with diffuse and polarization functions 6-31+G\* basis set<sup>23</sup> was employed for all calculations. The 60 lowest singlet excitation energies on the optimized geometry of  $[(L^{NO_2})Co^{III}(OMe)(H_2O)]$  (with a singlet spin state) in  $CH_3CN$  using the CPCM model<sup>24</sup> were calculated by the TD-DFT method.<sup>25</sup>

## RESULTS AND DISCUSSION

Details of the syntheses are presented in the [Experimental Section](#). The multicomponent redox reaction of  $L^R H_2$  with cobalt(II) salts in MeOH in the presence of triethylamine at room temperature affords  $OX_L^R$  in higher yields. The metal salts and solvents used, including the yields of the reactions, are summarized in Table 2. The  $^1H$  and  $^{13}C$  NMR spectra of  $OX_L^R$

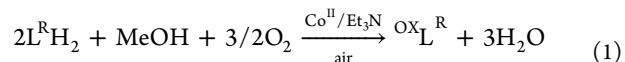
**Table 2.** Optimized Syntheses of  $OX_L^R$



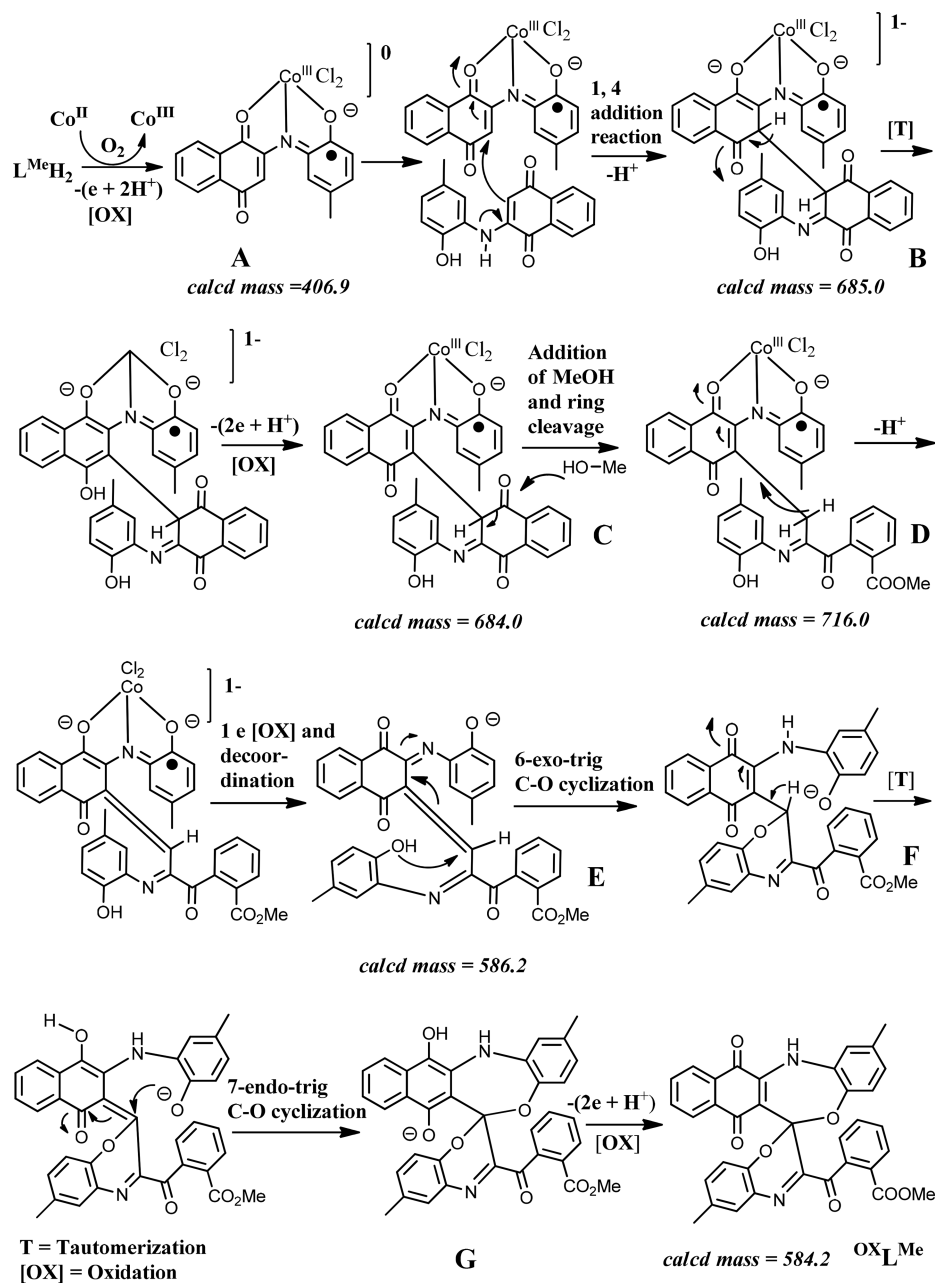
entry	$MX_2 \cdot 6H_2O$	solvent	R	$OX_L^R$	yield (%)
1	$CoCl_2 \cdot 6H_2O$	MeOH	H	$OX_L^H$	20
2	$Co(NO_3)_2 \cdot 6H_2O$	MeOH	H	$OX_L^H$	25
3	$CoCl_2 \cdot 6H_2O$	MeOH	Me	$OX_L^{Me}$	41
4	$Co(NO_3)_2 \cdot 6H_2O$	MeOH	Me	$OX_L^{Me}$	46
5	$CoCl_2 \cdot 6H_2O$	MeOH	$tBu$	$OX_L^{tBu}$	54
6	$Co(NO_3)_2 \cdot 6H_2O$	MeOH	$tBu$	$OX_L^{tBu}$	68

are illustrated in [Figures S1–S4](#) in the Supporting Information. The NMR shielding tensors and the spin–spin coupling constants are summarized in [Syntheses](#). The  $^1H$  NMR signals were assigned by comparing the  $^1H$  NMR spectra of  $OX_L^H$ ,  $OX_L^{Me}$ , and  $OX_L^{tBu}$ . The spectra of  $OX_L^{Me}$  and  $OX_L^{tBu}$  display three singlets. Two of them appear at 7.0–7.4 ppm and are absent in the case of  $OX_L^H$ . These signals are assigned to aromatic CH protons. The other singlet is observed at 8.3–8.4 ppm, which is present in all cases and is assigned to the NH proton. A similar singlet of such an NH proton in the  $^1H$  NMR spectra of a series of 1,4-naphthoquinone-based sulfonamides has been documented in the literature.<sup>26</sup>

The plausible intermediates of  $L^{Me}H_2 \rightarrow OX_L^{Me}$  conversions that were detected by ESI mass spectrometry are shown in [Scheme 2](#). The reaction mixture of  $L^{Me}H_2$  with  $CoCl_2$  and  $Et_3N$  in MeOH initially turned dark green and then slowly turned red, affording red crystals of  $OX_L^R$ . The overall reaction is given in [eq 1](#). In this reaction  $[(L^{Me})Co^{III}Cl_2]$  (A), obtained after oxidation of the  $[(L^{Me})Co^{II}]$  unit in air, is the active cascade precursor that conducts stepwise ( $6e + 6H^+$ ) oxidative dimerization of the ligand, where MeOH is a source of one proton and the ester function.



The formation of **A** was detected by peaks at  $m/z$  405, 406, and 407 (calculated exact mass 406.9) in the mass spectrum and an EPR signal at  $g = 2.008$ . The intermediate **A** was successfully isolated using  $CH_3CN$  as a solvent (*vide infra*). The ESI mass spectra of the reaction mixture were recorded at several intervals, and the spectra are shown in [Figures S5 and S6](#) in the Supporting Information. The peaks at  $m/z$  406 and 507

Scheme 2. Cascade Route of the Conversion  $L^{\text{Me}}\text{H}_2 \rightarrow \text{OX}L^{\text{Me}}$  Promoted by Cobalt Ion in MeOH

(dominant peak) corresponding to intermediates **A** and [**A** +  $\text{Et}_3\text{N}$ ] were detected from the green solution after 15 min of the reaction. **A** undergoes an electrophilic 1,4-addition reaction with  $L^{\text{Me}}\text{H}_2$ , resulting in the formation of the intermediate **B**, which undergoes tautomerization and two-electron-one-proton oxidation to intermediate **C**. The 1,4-addition reaction of the 1,4-naphthoquinone fragment in the presence of a transition-metal ion has also been documented in the literature.<sup>27</sup> The nucleophilic addition of MeOH to a nonconjugated  $\text{C}=\text{O}$  function of intermediate **C** leads to a ring cleavage reaction, affording **D**. This is an example of an aromatic ring cleavage reaction assisted by an alcohol. The aromatic ring cleavage is a subject of investigation in different aspects of bioinorganic chemistry,<sup>28</sup> and thus this observation is significant in chemical science. The peaks at  $m/z$  686 and 718 corresponding to the intermediates **B** and **D** were detected by ESI mass spectrometry (see Figure S6) of the reaction mixture

after 5 h. **D** undergoes deprotonation, one-electron oxidation, and decoordination to **E**. The pendant amidophenolato function of **E** promotes a 6-exo-trig C–O cyclization,<sup>29a</sup> generating the oxazine fragment **F**. **F** further undergoes tautomerization and a 7-endo-trig C–O coupling reaction<sup>29b</sup> (by a 1,4-proton shift) by another pendant phenolato function, furnishing an oxazepine moiety as in **G**. **G** is a hydroquinone derivative that undergoes two-electron-one-proton oxidation reaction in air and affords  $\text{OX}L^{\text{Me}}$ . 6-exo-trig C–O followed by 7-endo-trig C–O cyclizations that lead to an *p*-hydroquinone intermediate which undergoes easy oxidation to the product was considered preferable to 7-endo-trig C–O followed by 6-exo-trig C–O cyclization reactions that result in an *o*-amidophenolato intermediate. The calculated masses of **E**–**G** are similar to that of  $\text{OX}L^{\text{Me}}$  (calculated mass 584.2) and a stronger peak at  $m/z$  585 was detected in the ESI mass spectrum. The change in spectral features of the reaction

mixture in MeOH that exhibit several isosbestic points was recorded for a period of 3 h and is illustrated in Figure 1. The

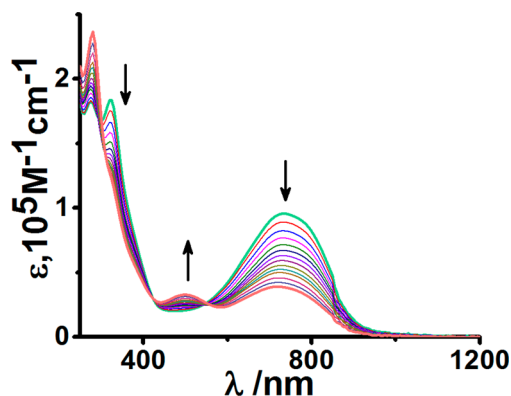


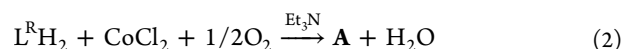
**Figure 1.** Changes in electronic spectra during  $L^{\text{Me}}\text{H}_2 \rightarrow \text{OXL}^{\text{Me}}$  conversion in MeOH in the presence of cobalt ion in air.

spectrum initially displays a lower energy absorption at 730 nm due to the radical intermediate **A**, which gradually disappears due to the formation of  $\text{OXL}^{\text{R}}$ , giving an absorption band at 505 nm (vide infra).

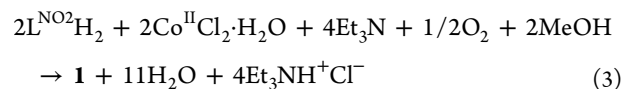
Notably, the yield of the reaction using cobalt nitrate is higher than that when cobalt chloride is used. This may be due to the easier decoordination of cobalt ion when nitrate is present as a coligand. The trend follows the spectrochemical series where nitrate is a weaker ligand than chloride. Semiquinonate anion radical complexes of cobalt(III) having chloride as coligands are numerous,<sup>30</sup> while stable semiquinonate anion radical complexes of cobalt(III) containing nitrate as a coligand have not been documented in the literature. Moreover, in this reaction cobalt ion is not a catalyst. After the first cycle of the reaction the de-coordinated cobalt is a solvated cobalt(III) ion, which is relatively inert. Thus, the coordination of cobalt(II) ion is preferred and the yield of the reaction containing a stoichiometric ratio of cobalt(II) salt and ligand was relatively higher than that when a catalytic amount of cobalt was used.

In this reaction MeOH acts as a reagent and is essential to yield a spiro derivative. No spiro derivative containing an ethyl ester as a functional group was successfully isolated from a reaction of  $L^{\text{Me}}\text{H}_2$  with cobalt salt in EtOH. One of the reasons is that MeOH is more acidic than EtOH and even more strongly acidic than water. For a successful reaction triethylamine and a solvent that can provide a proton is required. A similar reaction was performed in  $\text{CH}_3\text{CN}$ . The reaction does not yield the spiro product, but upon stirring for 2 h a green precipitate of **A** (see Figure S7 in the Supporting Information) separated out. The overall reaction in  $\text{CH}_3\text{CN}$  is given in eq 2. The search affirms that in both MeOH and  $\text{CH}_3\text{CN}$  the reaction proceeds via the intermediate **A**, which is less soluble

in  $\text{CH}_3\text{CN}$ . Notably, the reaction in a mixture of  $\text{CH}_3\text{CN}$  and MeOH solvents generates the spiro derivative. The same reaction under argon in MeOH does not furnish either any green solution or the spiro product, authenticating that air is an oxidant of this reaction where  $L^{\text{R}}\text{H}_2$  is oxidized to  $L^{\text{R}\bullet-}$  and cobalt(II) is oxidized to cobalt(III). This implies that the intermediate **A** containing an electron-deficient  $L^{\text{R}\bullet-}$  state coordinated to cobalt(III) ion promotes the cascade reaction. The role of triethylamine in this reaction is significant. In presence of triethylamine  $L^{\text{R}}\text{H}_2$  undergoes deprotonation, generating  $L^{\text{R}2-}$ , which coordinates cobalt(II) ion and further undergoes oxidation in the presence of air. In the absence of triethylamine no reaction of  $L^{\text{R}}\text{H}_2$  with a transition-metal ion occurs. In this particular reaction coordination of triethylamine to cobalt(III) ion stabilizing an intermediate was also detected (see Figure S5 in the Supporting Information). The driving force of the oxidative dimerization of the  $L^{\text{R}}\text{H}_2$  in MeOH is the formation of four covalent bonds in lieu of a cleavage of a C–C bond. It is noteworthy that formation of an ester, cleaving a C–C bond, is followed by two cyclization reactions involving two C–O bond formations. Overall the reaction progresses with the formation of a C–C bond and three C–O bonds with the production of three water molecules.

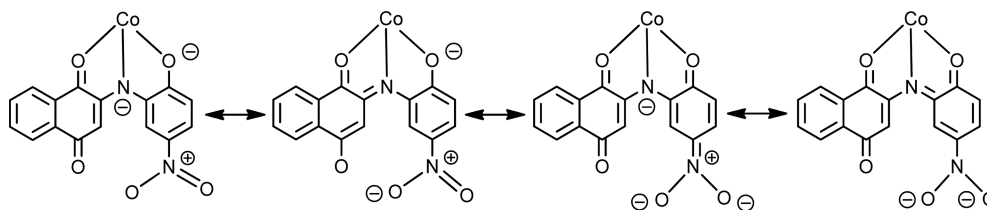


In the presence of an  $\text{NO}_2$  group the path of the reaction is different and no cascade was followed. The reaction of  $L^{\text{NO}_2}\text{H}_2$  with cobalt(II) salt affords **1**, following eq 3. No spiro derivative was isolated from this reaction. Isolation of **1** further confirmed the existence of cobalt(III) ion in the active precursor and supports the proposed path of the conversion of  $L^{\text{R}}\text{H}_2 \rightarrow \text{OXL}^{\text{R}}$ . Equation 3 also clarifies the significance of triethylamine in such a reaction involving *o*-aminophenol derivative as a ligand. In the presence of a  $-\text{NO}_2$  function the  $L^{\text{R}2-}$  chelate that exhibits several resonance structures as shown in Chart 2 was stabilized. The 1,4-addition reaction as proposed in Scheme 2 did not proceed, and the reaction furnishes the phenolato-bridged complex **1**.  $L^{\text{NO}_2}2-$  behaves more like a  $L^{\text{ONO}}\text{H}_3$  precursor, stabilizing the Cat-N-(1,4-naphthoquinone)(2-) state, while  $L^{\text{R}\bullet-}$  (R = H, Me, <sup>t</sup>Bu) becomes a cascade agent.



The success of the cascade reaction depends on the metal ion also coordinated to  $L^{\text{R}\bullet-}$ . The existence of the radical intermediate  $L^{\text{R}\bullet-}$  in the intermediate **A** was further established by isolating a dark bluish green  $L^{\text{R}\bullet-}$  complex of zinc(II) of the type  $[(L^{\text{Me}\bullet-})\text{Zn}^{\text{II}}\text{Cl}]$  (**2**) (see, Figure S8 in the Supporting Information) from a reaction of  $\text{ZnCl}_2$  and  $L^{\text{Me}}\text{H}_2$  in MeOH at room temperature. However, the reaction does not yield the spiro derivative.

**Chart 2.** Canonical Structures of  $[\text{Co}(L^{\text{NO}_2}2-)]$  Unit



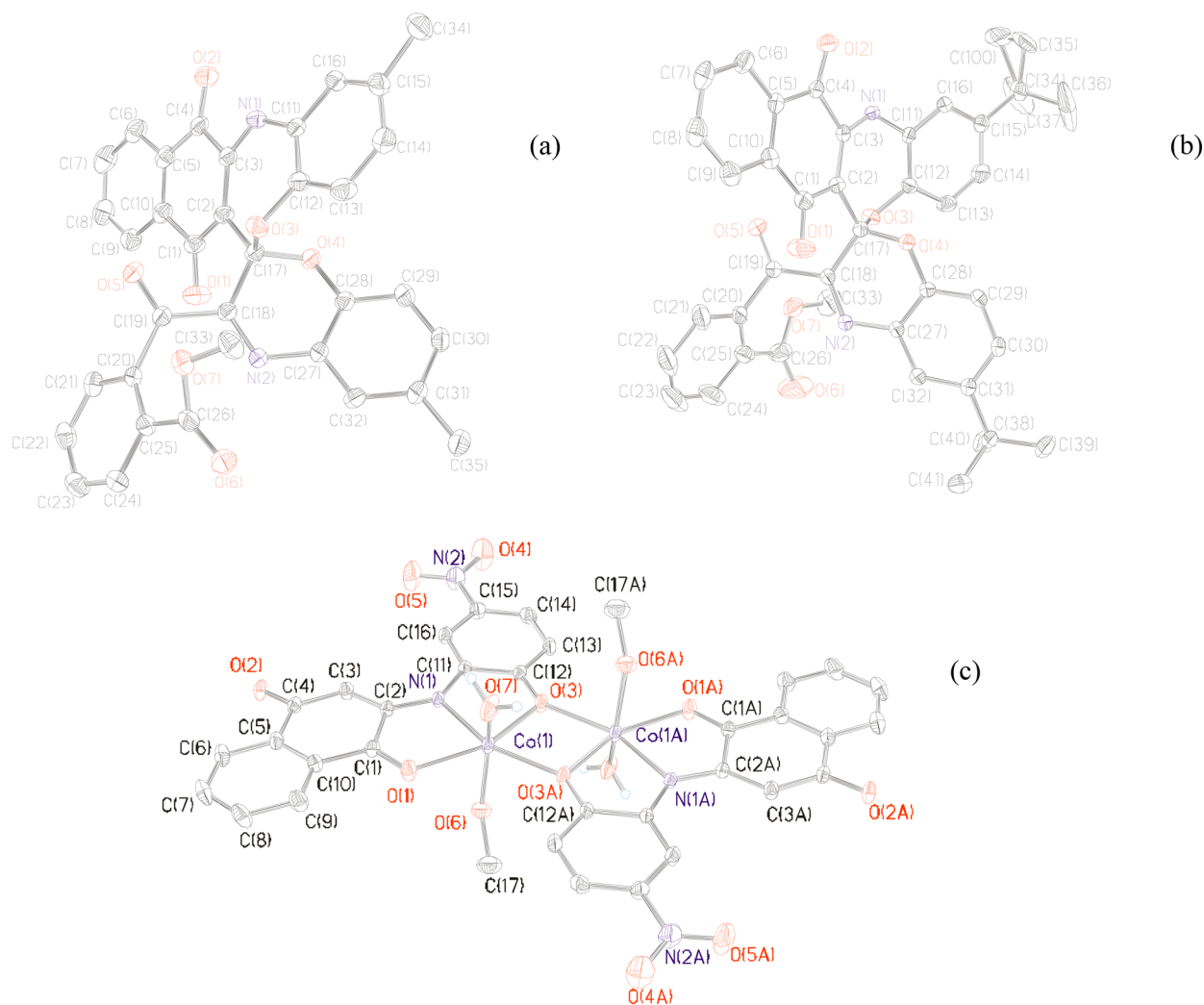


**Figure 2.** Molecular geometries of (a)  $\text{OXL}^{\text{Me}}$ , (b)  $\text{OXL}^{\text{tBu}}$ , and (c) **1** in the crystal state (40% thermal ellipsoids, hydrogen atoms omitted for clarity).

**Table 3.** Selected Experimental Bond Lengths (Å) and Angles (deg) of  $\text{OXL}^{\text{Me}}$ ,  $\text{OXL}^{\text{tBu}}$ , and **1**

	$\text{OXL}^{\text{Me}}$	$\text{OXL}^{\text{tBu}}$	<b>1</b>	
C(1)–O <sub>Q</sub>	1.237(7)	1.230(3)	C(1)–O(1)	1.232(3)
C(4)–O <sub>Q</sub>	1.211(7)	1.217(3)	C(4)–O(4)	1.284(3)
C(3)–N <sub>oxazepine</sub>	1.340(7)	1.354(3)	C(2)–N(1)	1.323(3)
C(11)–N <sub>oxazepine</sub>	1.403(8)	1.406(3)	C(11)–N(1)	1.401(4)
C(2)–C <sub>spiro</sub>	1.522(7)	1.509(3)	C(12)–O(3)	1.307(3)
C(18)–C <sub>spiro</sub>	1.514(7)	1.529(3)	C(15)–N(2)	1.453(4)
C <sub>spiro</sub> –O <sub>oxazepine</sub>	1.422(6)	1.424(3)	C(1)–C(2)	1.513(4)
C <sub>spiro</sub> –O <sub>oxazine</sub>	1.426(6)	1.428(3)	C(2)–C(3)	1.399(4)
C(18)–N <sub>oxazine</sub>	1.287(7)	1.283(3)	C(3)–C(4)	1.386(4)
C(27)–N <sub>oxazine</sub>	1.399(7)	1.402(3)	C(12)–C(11)	1.438(4)
C(2)–C(17)–O(3)	112.4(4)	114.11(19)	O(1)–Co(1)	2.135(3)
C(18)–C(17)–O(3)	101.6(4)	100.83(19)	N(1)–Co(1)	2.079(2)
O(3)–C(17)–O(4)	109.9(4)	109.69(19)	O(3)–Co(1)	2.044(2)
C(2)–C(17)–C(18)	116.5(5)	115.3(2)	O(6)–Co(1)	2.116(2)
O(4)–C(17)–C(18)	111.0(4)	111.19(19)	O(7)–Co(1)	2.051(3)
O(4)–C(17)–C(2)	105.4(4)	105.8(2)		

**X-ray Crystallography.** The molecular geometries of  $\text{OXL}^{\text{R}}$  were confirmed by the single-crystal X-ray structure determinations of  $\text{OXL}^{\text{Me}}$  and  $\text{OXL}^{\text{tBu}}$ . Similarly the molecular geometry of **1** in the crystal state was established by X-ray crystallography.

The crystallographic data are summarized in Table 1.  $\text{OXL}^{\text{Me}}$  and  $\text{OXL}^{\text{tBu}}$  crystallize respectively in  $P2_1/c$  and  $P\bar{1}$  space groups (CCDC 1561962–1561963). The molecular structures in the crystals and the atom labeling schemes of  $\text{OXL}^{\text{Me}}$  and  $\text{OXL}^{\text{tBu}}$  are

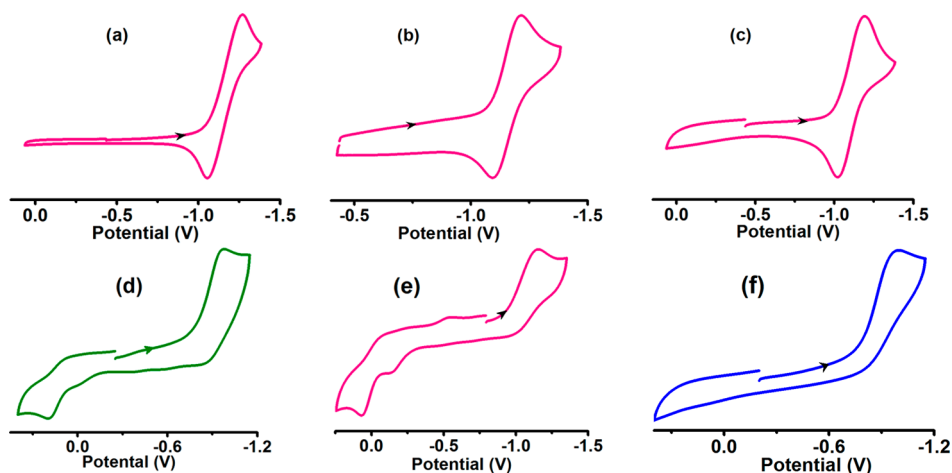


**Figure 3.** Cyclic voltammograms of (a)  $\text{OXL}^{\text{H}}$ , (b)  $\text{OXL}^{\text{Me}}$ , and (c)  $\text{OXL}^{\text{tBu}}$  in  $\text{CH}_2\text{Cl}_2$  (d) **A** in DMF. (e) **1** in  $\text{CH}_3\text{CN}$ . and (f) **2** in DMF at 298 K. Conditions: 0.2 M  $[\text{N}(n\text{-Bu})_4]\text{PF}_6$  supporting electrolyte; scan rate,  $100 \text{ mV s}^{-1}$ ; platinum working electrode.

illustrated in Figure 2a,b. The selected bond parameters are summarized in Table 3. The gross geometries and the selected bond parameters of  $\text{OXL}^{\text{Me}}$  and  $\text{OXL}^{\text{tBu}}$  are approximately similar. The bond parameters around the spiro carbon significantly deviate from the ideal values: e.g., the  $\text{C}(18)\text{--C}_{\text{spiro}}\text{--O}(3)$  angle is  $101.6(4)^\circ$  for  $\text{OXL}^{\text{Me}}$ . The average  $\text{C}_{\text{spiro}}\text{--O}_{\text{oxazine}}$  and  $\text{C}_{\text{spiro}}\text{--O}_{\text{oxazine}}$  lengths are  $1.423(6)$  and  $1.427(6)$  Å, respectively. The average  $\text{C}(3)\text{--N}_{\text{oxazine}}$  length,  $1.347(7)$  Å, is consistent with a  $\text{C}\text{--NH}$  single bond. Two  $\text{C}\text{--N}_{\text{oxazine}}$  lengths are significantly different. Because of the conjugation of the  $\text{--NH}$  with a  $\text{--C=O}$  group, the  $\text{C}(3)\text{--N}_{\text{oxazine}}$  lengths are relatively shorter. The shorter  $\text{C}(18)\text{--N}_{\text{oxazine}}$  length,  $1.285(5)$  Å, correlates to a  $\text{C=N}$  bond. The average  $\text{C}(27)\text{--N}_{\text{oxazine}}$  length is  $1.400(5)$  Å. The average  $\text{C=O}$  length of  $\text{OXL}^{\text{Me}}$  and  $\text{OXL}^{\text{tBu}}$  is  $1.224(4)$  Å.

**1** crystallizes in space group  $P2_1/n$  (CCDC 1561964). The molecular structure in the crystal state and the atom labeling scheme of **1** are depicted in Figure 2c. The selected bond parameters are summarized in Table 3. The octahedral coordination of the cobalt ion was achieved by bridging phenolato functions. The  $\text{C}\text{--O}$  and  $\text{C}\text{--N}$  lengths are consistent with the  $\text{Cat-N-(1,4-naphthoquinone)}$  state of the  $\text{L}^{\text{NO}_2^{2-}}$  ligand. The  $\text{C}(1)\text{--O}(1)$  and  $\text{C}(4)\text{--O}(2)$  lengths are  $1.232(3)$  and  $1.284(3)$  Å. The relatively longer  $\text{C}(11)\text{--N}(1)$  length,  $1.401(4)$  Å, is consistent with an amido-phenolato state of the  $\text{L}^{\text{NO}_2^{2-}}$  ligand. The  $\text{C}(12)\text{--O}(3)$  length is relatively shorter due to resonance with the nitro group, as shown in Chart 2. The  $\text{C}(2)\text{--N}(1)$  length,  $1.323(3)$  Å, is also shorter because of the resonance with one of the  $\text{C=O}$  functions. A similar trend is also noted in the cases of  $\text{OXL}^{\text{Me}}$  and  $\text{OXL}^{\text{tBu}}$ . The  $\text{Co}^{\text{III}}\text{--N}$  length is  $2.079(2)$  Å. The  $\text{Co}^{\text{III}}\text{--O}_{\text{Q}}$  length is expectedly longer than the  $\text{Co}^{\text{III}}\text{--O}_{\text{phenolato}}$  length. The  $\text{Co}^{\text{III}}\text{--OMe}$  length is  $2.092(2)$  Å and is similar to those reported in other cobalt(III) complexes.<sup>31</sup>

**Redox Activity and Electron Paramagnetic Resonance (EPR) and UV–Vis–NIR Absorption Spectra.** The  $\text{OXL}^{\text{R}}$  derivatives are redox active and exhibit a reversible cathodic wave at  $-1.1$  V referenced to the  $\text{Fc}/\text{Fc}^+$  couple as shown in Figure 3a–c, due to the 1,4-naphthoquinone/1,4-naphthoquinone redox couple. The corresponding redox wave of **1** as depicted in Figure 3e is irreversible. **1** also exhibits two successive anodic peaks, respectively, at  $-0.14$  and  $0.07$  V due to the  $\text{SQ-N-(1,4-naphthoquinone)}/\text{Cat-N-(1,4-naphthoquinone)}$

redox couples. The redox activity of the cascade precursor **A** is notably different from those of  $\text{OXL}^{\text{R}}$  and **1**. The cyclic voltammogram of **A** displays one reversible anodic wave at  $+0.14$  V, as shown in Figure 3d, due to the  $\text{L}^{\text{R}\bullet\text{--}}/\text{L}^{\text{R}0}$  redox couple. In the case of **2**, no such anodic wave was recorded and the cathodic wave due to the  $\text{L}^{\text{R}\bullet\text{--}}/\text{L}^{\text{R}2\text{--}}$  redox couple is irreversible (see Figure 3f).

The X-band EPR spectrum of the powder sample of **A** that exhibits a strong signal at  $g = 2.008$  at room temperature is shown in Figure 4a. The spectrum displays hyperfine splitting

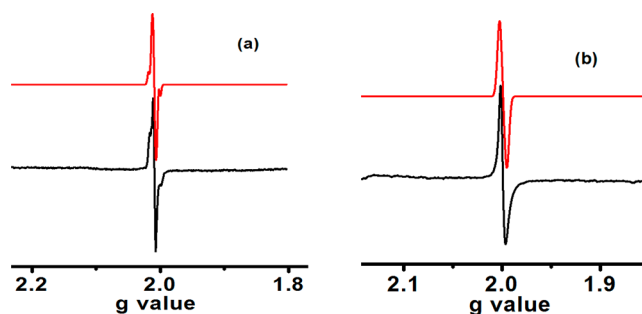


**Figure 4.** X-band EPR spectra of (a) **A** (powder) and (b) **2** (powder) at 298 K (experimental, black; simulated, red).

( $A_{\text{N}} = 13.1$  G) due to  $^{14}\text{N}$  nuclei ( $I = 1$ ). The EPR spectrum of the DMF solution is similar to that of the powder sample. No shift of the charge from the ligand to metal was observed even in a frozen glass at 110 K, confirming the existence of  $\text{L}^{\text{R}\bullet\text{--}}$  coordinated to low-spin cobalt(III) ion in **A**. The similar EPR spectrum of the mass obtained after evaporation of the resulting green solution of the reaction of cobalt(II) chloride with  $\text{L}^{\text{Me}}\text{H}_2$  in MeOH in air was recorded, confirming the formation of radical intermediate **A** in the reaction. The EPR spectra of the powder sample and a DMF solution of **2** are similar to that of **A**, as depicted in Figure 4b. The simulated  $g$  value is 1.999, which authenticates the coordination of  $\text{L}^{\text{R}\bullet\text{--}}$  with zinc(II) ion in **2**.

The UV–vis–NIR absorption spectra of  $\text{L}^{\text{R}}\text{H}_2$  and  $\text{OXL}^{\text{R}}$  as depicted in Figure 5 were recorded in  $\text{CH}_2\text{Cl}_2$ , while the spectrum of **1** was recorded in  $\text{CH}_3\text{CN}$ . The spectral data are summarized in Table 4. The spectra of  $\text{OXL}^{\text{R}}$  ( $\text{R} = \text{H}, \text{Me}, \text{tBu}$ ) derivatives display a characteristic absorption band at 505 nm.

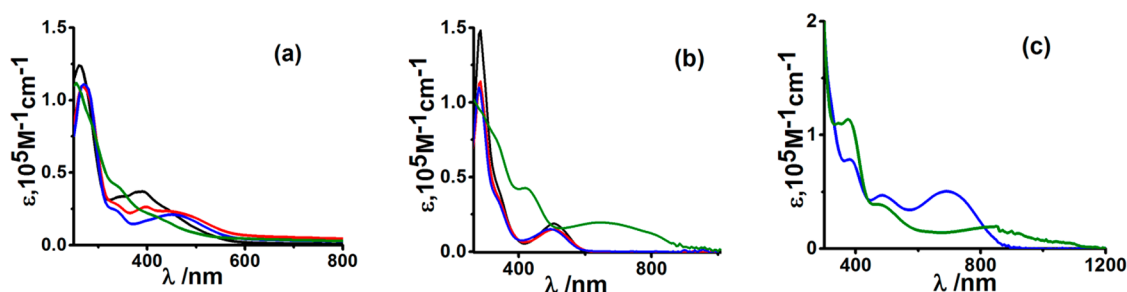


**Figure 5.** UV-vis/NIR absorption spectra of (a)  $L^H_2$  (black),  $L^{Me}_2$  (red),  $L^{tBu}_2$  (blue), and  $L^{NO_2}_2$  (green), (b)  $OXL^H$  (blue),  $OXL^{Me}$  (red), and  $OXL^{tBu}$  (black) in  $CH_2Cl_2$  and **1** (green) in  $CH_3CN$ , and (c) **A** (green) and **2** (blue) in DMF at 298 K.

**Table 4.** UV-Vis-NIR Absorption Spectral Data of  $L^R_2$  ( $R = -Me, -tBu, -NO_2$ ),  $OXL^H$ ,  $OXL^{Me}$ ,  $OXL^{tBu}$ , **1**, **A**, and **2** at 298 K

compound	solvent	$\lambda_{max}$ nm ( $\epsilon$ , $10^5 M^{-1} cm^{-1}$ )
$L^H_2$	$CH_2Cl_2$	440 (0.25), 392 (0.37), 371 (0.36), 338 (0.34), 279 (1.25)
$L^{Me}_2$	$CH_2Cl_2$	496 (0.19), 452 (0.23), 397 (0.26), 334 (0.29), 285 (0.97)
$L^{tBu}_2$	$CH_2Cl_2$	450 (0.21), 335 (0.24), 284 (1.00), 271 (1.11)
$L^{NO_2}_2$	$CH_2Cl_2$	443 (0.15), 420 (0.19), 342 (0.40), 285 (0.86)
$OXL^H$	$CH_2Cl_2$	499 (0.15), 335 (0.35), 279 (1.09)
$OXL^{Me}$	$CH_2Cl_2$	508 (0.15), 343 (0.34), 284 (1.13)
$OXL^{tBu}$	$CH_2Cl_2$	506 (0.19), 344 (0.39), 284 (1.47)
<b>A</b>	DMF	820 (0.20), 480 (0.39), 370 (1.30), 342 (1.19)
<b>1</b>	$CH_3CN$	790 (0.13), 654 (0.20), 424 (0.42), 336 (0.73)
<b>2</b>	DMF	700 (0.50), 480 (0.47), 380 (0.78)

Notably,  $OXL^R$  species are weakly fluorescent. The excitation and emission wavelengths are given in Table S1 in the Supporting Information. Excitations of  $OXL^R$  at 337–340 nm emit at 380 nm with quantum yields of lower than 0.01%. The selected excitation and emission spectra of  $OXL^R$  are shown in Figure S9 in the Supporting Information. The electronic spectrum of **1** displays a broader NIR absorption band at 500–900 nm.

The origin of this NIR band was investigated by the TD DFT calculations on the mononuclear  $[(L^{NO_2_2})Co^{III}(OMe)(H_2O)]$  unit in  $CH_3CN$  using the CPCM model. The calculated wavelengths ( $\lambda_{cal}$ ) and the oscillation strengths ( $f$ ) of the significant transitions are summarized in Table S2 in the Supporting Information. The NIR  $\lambda_{cal}$  value with  $f = 0.089$  is 768.95 nm, which is due to an *o*-amidophenolato (HOMO)  $\rightarrow \pi_Q^*$  (LUMO) transition (91%). Thus, the NIR absorption of **1** at 650–700 nm ( $\lambda_{ex}$ ) is assigned to a spin-allowed closed-shell singlet to open-shell singlet ILCT transition. The NIR band is absent in  $OXL^R$  derivatives. The UV-vis-NIR absorption spectra of **A** and **2** containing  $L^{R\bullet-}$  display a lower energy absorption band, as shown in Figure 5c. In DMF **A** exhibits a NIR band at 820 nm, while the NIR band of **2** appears at 700 nm due to an ILCT transition. Notably the initial green solution of MeOH containing intermediate **A** of the reaction of cobalt chloride and  $L^R_2$  exhibits a strong NIR band at 730 nm (see Figure 1).

## CONCLUSION

The biofunctionality of a molecule that contains both oxazine and oxazepine fragments has been the subject of investigation. However, no such molecule has been reported so far. In this study, a family of spiro oxazine-oxazepine derivatives which are

isolated from an unprecedented cascade route is disclosed. The reaction of cobalt(II) chloride with *N*-(1,4-naphthoquinone)-*o*-aminophenol derivatives ( $L^R_2$ ) in MeOH promotes a redox cascade, producing oxazine-oxazepine derivatives ( $R = H, Me, tBu$ ) in good yields. The cascade precursor is  $[(L^{Me\bullet-})Co^{III}Cl_2]$  (**A**) obtained after  $(2e + 2H^+)$  oxidation of  $[(L^{Me2-})Co^{II}]$  unit in air. The  $(6e + 6H^+)$  oxidative dimerization of  $L^R_2$  is composed of C–C bond formation, C–C bond cleavage, and 6-exo-trig and 7-endo-trig cyclizations based on C–O coupling reactions, where MeOH is the source of a proton and the ester function. Both the route (with minimum chemical waste and higher atomic economy) and the product are useful in pharmacy in designing broad-spectrum drugs. Notably, the route of the reaction is tunable by *R*. No cascade progresses when  $R = NO_2$ , and the  $(2e + 4H^+)$  oxidation reaction ends, furnishing a dinuclear cobalt(III) complex that stabilizes a Cat-N-(1,4-naphthoquinone)(2-) state. The reaction also depends on the solvent and the metal ion used. In  $CH_3CN$  it gives only **A**, while the reaction in MeOH with zinc(II) ion affords a stable  $L^{R\bullet-}$  complex,  $[(L^{Me\bullet-})Zn^{II}Cl]$  (**2**). The study implies that the redox activity of  $L^R_2$  containing a (phenol)-NH-(1,4-naphthoquinone) fragment is notably different from that of a (phenol)-NH-(phenol) precursor. The former can be used as a cascade precursor, while the latter generates complexes that exhibit VT.

## ASSOCIATED CONTENT

### Supporting Information

The Supporting Information is available free of charge on the ACS Publications website at DOI: 10.1021/acs.inorgchem.7b01961.

$^1H$  and  $^{13}C$  NMR spectra, ESI mass spectra, excitation and emission wavelengths, excitation energies, oscillator strengths, transition types, and dominant contributions of UV-vis-NIR absorption bands obtained from TD DFT calculations, and gas-phase optimized coordinates (PDF)

### Accession Codes

CCDC 1561962–1561964 contain the supplementary crystallographic data for this paper. These data can be obtained free of charge via [www.ccdc.cam.ac.uk/data\\_request/cif](http://www.ccdc.cam.ac.uk/data_request/cif), or by emailing [data\\_request@ccdc.cam.ac.uk](mailto:data_request@ccdc.cam.ac.uk), or by contacting The Cambridge Crystallographic Data Centre, 12 Union Road, Cambridge CB2 1EZ, UK; fax: +44 1223 336033.

## AUTHOR INFORMATION

### Corresponding Author

\*P.G.: e-mail, [ghosh@pghosh.in](mailto:ghosh@pghosh.in); tel, +91-33-2428-7347; fax, +91-33-2477-3597.

ORCID 

Prasanta Ghosh: 0000-0002-2925-1802

## Notes

The authors declare no competing financial interest.

## ACKNOWLEDGMENTS

Financial support received from the University Grants Commission (F. No. 43-214/2014(SR)), SERB-DST, New Delhi (EMR/2016/005222), and WB-DST, India, is gratefully acknowledged. S.M. is grateful to the UGC, New Delhi, India, for a fellowship (F. No. 11-24/2013 (SA-1) dated 08.07.1014).

## REFERENCES

- (1) Simpson, C. L.; Boone, S. R.; Pierpont, C. G. Charge Distribution in Transition-Metal Complexes of a Schiff Base Biquinone Ligand. Structural and Electrochemical Properties of the  $M^{II}(\text{Cat-N-BQ})$ ,  $M^{III}(\text{Cat-N-BQ})(\text{Cat-N-SQ})$ ,  $M^{IV}(\text{Cat-N-SQ})_2$  Tautomeric Series. *Inorg. Chem.* **1989**, *28*, 4379–4385.
- (2) Chaudhuri, P.; Hess, M.; Hildebrand, K.; Bill, E.; Weyhermüller, T.; Wieghardt, K. Ligand-Based Redox Isomers of  $[\text{Zn}^{II}(\text{C}_{28}\text{H}_{40}\text{NO}_2)_2]$ : Molecular and Electronic Structures of a Diamagnetic Green and a Paramagnetic Red Form. *Inorg. Chem.* **1999**, *38*, 2781–2790.
- (3) (a) Wong, J. L.; Higgins, R. F.; Bhowmick, I.; Cao, D. X.; Szigethy, G.; Ziller, J. W.; Shores, M. P.; Heyduk, A. F. Bimetallic iron–iron and iron–zinc complexes of the redox-active ONO pincer ligand. *Chem. Sci.* **2016**, *7*, 1594–1599. (b) Broere, D. L. J.; Plessius, R.; van der Vlugt, J. I. New avenues for ligand-mediated processes—expanding metal reactivity by the use of redox-active catechol, o-aminophenol and o-phenylenediamine ligands. *Chem. Soc. Rev.* **2015**, *44*, 6886–6915. (c) Szigethy, G.; Shaffer, D. W.; Heyduk, A. F. Coordination Effects on Electron Distributions for Rhodium Complexes of the Redox-Active Bis(3,5-di-tert-butyl-2-phenolate)-amide Ligand. *Inorg. Chem.* **2012**, *51*, 12606–12618.
- (4) Mondal, M. K.; Tiwari, A.; Mukherjee, C. A Solid-State Valence Tautomeric Octahedral  $\{\text{Co}^{II}(\text{BQ}_2\text{-N-Cat})\}_0$  Complex Formation via Ligand-Centered Phenolic C–O Bond breaking and Co–O Bond making. *Chem. Commun.* **2016**, *52*, 11995–11998.
- (5) (a) Novio, F.; Evangelio, E.; Vazquez-Mera, N.; González-Monje, P.; Bellido, E.; Mendes, S.; Kehagias, N.; Ruiz-Molina, D. Robust spin crossover platforms with synchronized spin switch and polymer phase transition. *Sci. Rep.* **2013**, *3*, 1708. (b) Cador, O.; Chabre, F.; Dei, A.; Sangregorio, C.; Slagere, J. V.; Vaz, M. G. F. Temperature-Induced Solid-State Valence Tautomeric Interconversion in Two Cobalt–Schiff Base Diquinone Complexes. *Inorg. Chem.* **2003**, *42*, 6432–6440.
- (6) (a) Ngo, T. A.; Nakata, E.; Saimura, M.; Morii, T. Spatially organized enzymes drive cofactor-coupled cascade reactions. *J. Am. Chem. Soc.* **2016**, *138*, 3012. (b) Han, B.; Huang, W.; Ren, W.; He, G.; Wang, J.-h.; Peng, C. Asymmetric Synthesis of Cyclohexane-Fused Drug-Like Spirocyclic Scaffolds Containing Six Contiguous Stereogenic Centers via Organocatalytic Cascade Reactions. *Adv. Synth. Catal.* **2015**, *357*, 561. (c) Lonca, G. H.; Tejo, C.; Chan, H. L.; Chiba, S.; Gagosz, F. Gold(I)-Catalyzed 6-endo-dig Azide-Yne Cyclization: an Efficient Access to 2H-1,3-Oxazines. *Chem. Commun.* **2017**, *53*, 736.
- (7) (a) Lu, L.-Q.; Chen, J.-R.; Xiao, W.-J. Development of Cascade Reactions for the Concise Construction of Diverse Heterocyclic Architectures. *Acc. Chem. Res.* **2012**, *45*, 1278–1294. (b) Grondal, C.; Jeanty, M.; Enders, D. Organocatalytic cascade reactions as a new tool in total synthesis. *Nat. Chem.* **2010**, *2*, 167–178. (c) Yeom, H. S.; Lee, Y.; Jeong, J.; So, E.; Hwang, S.; Lee, J. E.; Lee, S. S.; Shin, S. Stereoselective One-Pot Synthesis of 1-Aminoindanes and 5,6-Fused Azacycles Using a Gold-Catalyzed Redox-Pinacol-Mannich-Michael Cascade. *Angew. Chem., Int. Ed.* **2010**, *49*, 1611–1614.
- (8) (a) Nakamura, I.; Kudo, Y.; Terada, M. Oxazepine Synthesis by Copper-Catalyzed Intermolecular Cascade Reactions between O-Propargylic Oximes and Dipolarophiles. *Angew. Chem., Int. Ed.* **2013**, *52*, 7536. (b) Vandavasi, J. K.; Hu, W. P.; Chen, H. Y.; Senadi, G. C.; Chen, C. Y.; Wang, J. J. A New Approach to 1,4-Oxazines and 1,4-Oxazepines via Base-Promoted Exo Mode Cyclization of Alkynyl Alcohols: Mechanism and DFT Studies. *Org. Lett.* **2012**, *14*, 3134–3137.
- (9) (a) Mao, X. F.; Zhu, X. P.; Li, D. Y.; Liu, P. N. Cu-Catalyzed Cascade Annulation of Alkynols with 2-Azidobenzaldehydes: Access to 6H-Isocromeno[4,3-c]quinoline. *J. Org. Chem.* **2017**, *82*, 7032–7039. (b) Ko, Y. O.; Jeon, H. J.; Jung, D. J.; Kim, U. B.; Lee, S.-g. Rh(II)/Mg(OtBu)<sub>2</sub>-Catalyzed Tandem One-Pot Synthesis of 1,4-Oxazepines and 1,4-Oxazines from N-Sulfonyl-1,2,3-triazoles and Glycidols. *Org. Lett.* **2016**, *18*, 6432–6435. (c) Nicolaou, K. C.; Chen, J. S. The art of total synthesis through cascade reactions. *Chem. Soc. Rev.* **2009**, *38*, 2993–3009.
- (10) Zhang, Y.; Ye, S.; Ji, M.; Li, L.; Guo, D.; Zhu, G. Copper-Catalyzed Radical Cascade Difluoromethylation/Cyclization of 2-(3-Arylpropionyl)benzaldehydes: A Route to Difluoromethylated Naphthoquinones. *J. Org. Chem.* **2017**, *82*, 6811–6818.
- (11) Mondal, S.; Maity, S.; Ghosh, P. A Redox-Active Cascade Precursor: Isolation of a Zwitterionic Triphenylphosphonio–Hydrazyl Radical and an Indazolo–Indazole Derivative. *Inorg. Chem.* **2017**, *56*, 8878–8888.
- (12) (a) Palmer, B. D.; Sutherland, H. S.; Blaser, A.; Kmentova, I.; Franzblau, S. G.; Wan, B.; Wang, Y.; Ma, Z.; Denny, W. A.; Thompson, A. M. Synthesis and Structure–Activity Relationships for Extended Side Chain Analogues of the Antitubercular Drug (6S)-2-Nitro-6-[[4-(trifluoromethoxy)benzyl]oxy]-6,7-dihydro-5H-imidazo[2,1-b][1,3]oxazine (PA-824). *J. Med. Chem.* **2015**, *58*, 3036. (b) Ladopoulou, E.; Matralis, A. N.; Kourounakis, A. P. New Multifunctional Di-tert-butylphenol octahydro(pyrido/benz)oxazine Derivatives with Antioxidant, Antihyperlipidemic, and Antidiabetic Action. *J. Med. Chem.* **2013**, *56*, 3330–3339. (c) Abou-Elmagd, W. S. I.; Hashem, A. I. Synthesis of 1-amidoalkyl-2-naphthols and oxazine derivatives with study of their antibacterial and antiviral activities. *Med. Chem. Res.* **2013**, *22*, 2005–2013. (d) Verma, V.; Singh, K.; Kumar, D.; Klapötke, T. M.; Stierstorfer, J.; Narasimhan, B.; Qazi, A. K.; Hamid, A.; Jaglan, S. Synthesis, antimicrobial and cytotoxicity study of 1,3-disubstituted-1H-naphtho[1,2-e][1,3]oxazines. *Eur. J. Med. Chem.* **2012**, *56*, 195–202. (e) Tang, Z.; Chen, W.; Zhu, Z.; Liu, H. Synthesis of 2,3-Diaryl-3,4-dihydro-2H-1,3-benzoxazines and Their Fungicidal Activities. *J. Heterocyclic Chem.* **2011**, *48*, 255–260. (f) Basappa; Murugan, S.; Kavitha, C. V.; Purushothaman, A.; Nevin, K. G.; Sugahara, K.; Rangappa, K. S. A small oxazine compound as an anti-tumor agent: A novel pyranoside mimetic that binds to VEGF, HB-EGF, and TNF- $\alpha$ . *Cancer Lett.* **2010**, *297*, 231–243. (g) Das, B. C.; Madhukumar, A. V.; Anguiano, J.; Mani, S. Design, synthesis and biological evaluation of 2H-benzo[b][1,4] oxazine derivatives as hypoxia targeted compounds for cancer therapeutics. *Bioorg. Med. Chem. Lett.* **2009**, *19*, 4204–4206.
- (13) (a) Yang, D.; Wan, C.; He, M.; Che, C.; Xiao, Y.; Fu, B.; Qin, Z. Design, synthesis, crystal structure and fungicidal activity of (E)-5-(methoxyimino)-3,5-dihydrobenzo[e][1,2]oxazepin-4(1H)-one analogues. *MedChemComm* **2017**, *8*, 1366–1373. (b) Blass, B. 5-Amino-oxazepine and 5-Amino-thiazepine Compounds as  $\beta$ -Secretase Antagonists and Methods of Use. *ACS Med. Chem. Lett.* **2012**, *3*, 873–874. (c) Deng, X. Q.; Wei, C. X.; Li, F. N.; Sun, Z. G.; Quan, Z. S. Design and synthesis of 10-alkoxy-5, 6-dihydro-triazolo[4,3-d]benzo[f][1,4]oxazepine derivatives with anticonvulsant activity. *Eur. J. Med. Chem.* **2010**, *45*, 3080–3086.
- (14) Castaldi, G.; Allegrini, P. Photocromatic and thermocromatic spiro oxazine-oxazepine compounds and the process for their preparation. U.S. Patent US5171636 A, 1992.
- (15) (a) Sheldrick, G. M. A short history of SHELX. *Acta Crystallogr., Sect. A: Found. Crystallogr.* **2008**, *64*, 112–122. (b) Sheldrick, G. M. Crystal structure refinement with SHELXL. *Acta Crystallogr., Sect. C: Struct. Chem.* **2015**, *71*, 3–8.
- (16) Frisch, M. J.; Trucks, G. W.; Schlegel, H. B.; Scuseria, G. E.; Robb, M. A.; Cheeseman, J. R.; Montgomery, J. A., Jr.; Vreven, T.; Kudin, K. N.; Burant, J. C.; Millam, J. M.; Iyengar, S. S.; Tomasi, J.; Barone, V.; Mennucci, B.; Cossi, M.; Scalmani, G.; Rega, N.;

Petersson, G. A.; Nakatsuji, H.; Hada, M.; Ehara, M.; Toyota, K.; Fukuda, R.; Hasegawa, J.; Ishida, M.; Nakajima, T.; Honda, Y.; Kitao, O.; Nakai, H.; Klene, M.; Li, X.; Knox, J. E.; Hratchian, H. P.; Cross, J. B.; Bakken, V.; Adamo, C.; Jaramillo, J.; Gomperts, R.; Stratmann, R. E.; Yazyev, O.; Austin, A. J.; Cammi, R.; Pomelli, C.; Ochterski, J. W.; Ayala, P. Y.; Morokuma, K.; Voth, G. A.; Salvador, P.; Dannenberg, J. J.; Zakrzewski, V. G.; Dapprich, S.; Daniels, A. D.; Strain, M. C.; Farkas, O.; Malick, D. K.; Rabuck, A. D.; Raghavachari, K.; Foresman, J. B.; Ortiz, J. V.; Cui, Q.; Baboul, A. G.; Clifford, S.; Cioslowski, J.; Stefanov, B. B.; Liu, G.; Liashenko, A.; Piskorz, P.; Komaromi, I.; Martin, R. L.; Fox, D. J.; Keith, T.; Al-Laham, M. A.; Peng, C. Y.; Nanayakkara, A.; Challacombe, M.; Gill, P. M. W.; Johnson, B.; Chen, W.; Wong, M. W.; Gonzalez, C.; Pople, J. A. *Gaussian 03, revision E.01*; Gaussian, Inc., Wallingford, CT, 2004.

(17) (a) Parr, R. G.; Yang, W. *Density Functional Theory of Atoms and Molecules*; Oxford University Press: Oxford, U.K., 1989. (b) Salahub, D. R.; Zerner, M. C. *The Challenge of d and f Electrons*; American Chemical Society: Washington, DC, 1989; ACS Symposium Series 394. (c) Kohn, W.; Sham, L. Self-Consistent Equations Including Exchange and Correlation Effects. *Phys. Rev.* **1965**, *140*, A1133–A1138. (d) Hohenberg, P.; Kohn, W. Inhomogeneous Electron Gas. *Phys. Rev.* **1964**, *136*, B864–B871.

(18) (a) Becke, A. D. Density-functional thermochemistry. III. The Role of Exact Exchange. *J. Chem. Phys.* **1993**, *98*, 5648–5652. (b) Miehlich, B.; Savin, A.; Stoll, H.; Preuss, H. Results Obtained with the Correlation Energy Density Functionals of Becke and Lee, Yang and Parr. *Chem. Phys. Lett.* **1989**, *157*, 200–206. (c) Lee, C.; Yang, W.; Parr, R. G. Development of the Colle-Salvetti Correlation-Energy Formula into a Functional of the Electron Density. *Phys. Rev. B: Condens. Matter Mater. Phys.* **1988**, *37*, 785–789.

(19) Pulay, P. Improved SCF Convergence Acceleration. *J. Comput. Chem.* **1982**, *3*, 556–560.

(20) Schlegel, H. B.; McDouall, J. J. In *Computational Advances in Organic Chemistry*; Ogretir, C., Csizmadia, I. G., Eds.; Kluwer Academic: Dordrecht, The Netherlands, 1991; pp 167–185.

(21) (a) Hay, P. J.; Wadt, W. R. Ab Initio Effective Core Potentials for Molecular Calculations. Potentials for the Transition Metal Atoms Sc to Hg. *J. Chem. Phys.* **1985**, *82*, 270–283. (b) Wadt, W. R.; Hay, P. J. Ab Initio Effective Core Potentials for Molecular Calculations. Potentials for Main Group Elements Na to Bi. *J. Chem. Phys.* **1985**, *82*, 284–298. (c) Hay, P. J.; Wadt, W. R. A. Ab Initio Effective Core Potentials for Molecular Calculations. Potentials for K to Au including the Outermost Core Orbitals. *J. Chem. Phys.* **1985**, *82*, 299–310.

(22) (a) Rassolov, V. A.; Ratner, M. A.; Pople, J. A.; Redfern, P. C.; Curtiss, L. A. 6-31G\* Basis Set for Third-row Atoms. *J. Comput. Chem.* **2001**, *22*, 976–984. (b) Francl, M. M.; Pietro, W. J.; Hehre, W. J.; Binkley, J. S.; DeFrees, D. J.; Pople, J. A.; Gordon, M. S. Self-Consistent Molecular Orbital Methods. 23. A Polarization Basis Set for Second Row Elements. *J. Chem. Phys.* **1982**, *77*, 3654–3665. (c) Hariharan, P. C.; Pople, J. A. Accuracy of AHn Equilibrium Geometries by Single Determinant Molecular Orbital Theory. *Mol. Phys.* **1974**, *27*, 209–214. (d) Hariharan, P. C.; Pople, J. A. The Influence of Polarization Functions on Molecular Orbital Hydrogenation Energies. *Theor. Chim. Acta.* **1973**, *28*, 213–222.

(23) Hehre, W. J.; Ditchfield, R.; Pople, J. A. A. Self-Consistent Molecular Orbital Methods. XII. Further Extensions of Gaussian-Type Basis Sets for Use in Molecular Orbital Studies of Organic Molecules. *J. Chem. Phys.* **1972**, *56*, 2257–2261.

(24) (a) Cossi, M.; Rega, N.; Scalmani, G.; Barone, V. Energies, Structures, and Electronic Properties of Molecules in Solution with the CPCM Solvation Model. *J. Comput. Chem.* **2003**, *24*, 669–681. (b) Barone, V.; Cossi, M. Quantum Calculation of Molecular Energies and Energy Gradients in Solution by a Conductor Solvent Model. *J. Phys. Chem. A* **1998**, *102*, 1995–2001.

(25) (a) Stratmann, R. E.; Scuseria, G. E.; Frisch, M. An Efficient Implementation of Time-Dependent Density-Functional Theory for the Calculation of Excitation Energies of Large Molecules. *J. Chem. Phys.* **1998**, *109*, 8218–8224. (b) Casida, M. E.; Jamorski, C.; Casida, K. C.; Salahub, D. R. Molecular Excitation Energies to High-lying

Bound States from Time-Dependent Density-Functional Response Theory: Characterization and Correction of the Time Dependent Local Density Approximation Ionization Threshold. *J. Chem. Phys.* **1998**, *108*, 4439–4449. (c) Bauernschmitt, R.; Ahlrichs, R. Treatment of Electronic Excitations within the Adiabatic Approximation of Time Dependent Density Functional Theory. *Chem. Phys. Lett.* **1996**, *256*, 454–464.

(26) Prachayasittikul, V.; Pingaew, R.; Worachartcheewan, A.; Nantasenamat, C.; Prachayasittikul, S.; Ruchirawat, S.; Prachayasittikul, V. Novel 1,4-naphthoquinone-based sulfonamides: synthesis, QSAR, anticancer and antimalarial studies. *Eur. J. Med. Chem.* **2014**, *84*, 247–263.

(27) Liu, Y.; Sun, J.-W. Copper(II)-Catalyzed Synthesis of Benzo-[f]pyrido[1,2-a]indole-6,11-dione Derivatives via Naphthoquinone Difunctionalization Reaction. *J. Org. Chem.* **2012**, *77*, 1191–1197.

(28) Paul, G. C.; Banerjee, S.; Mukherjee, C. Dioxygen Reactivity of an Iron Complex of 2-Aminophenol-Appended Ligand: Crystallographic Evidence of the Aromatic Ring Cleavage Product of the 2-Aminophenol Unit. *Inorg. Chem.* **2017**, *56*, 729–736. (b) Maity, S.; Kundu, S.; Mondal, S.; Bera, S.; Ghosh, P. Molecular and Electronic Structures of Ruthenium Complexes Containing an ONS-Coordinated Open-Shell  $\pi$  Radical and an Oxidative Aromatic Ring Cleavage Reaction. *Inorg. Chem.* **2017**, *56*, 3363–3376. (c) Chatterjee, S.; Paine, T. K. Oxygenative Aromatic Ring Cleavage of 2-Aminophenol with Dioxygen Catalyzed by a Nonheme Iron Complex: Catalytic Functional Model of 2-Aminophenol Dioxygenases. *Inorg. Chem.* **2015**, *54*, 1720–1727.

(29) (a) Kishore Vandavasi, J.; Hu, W.-P.; Senadi, G. C.; Chen, H.-T.; Chen, H.-Y.; Hsieh, K.-C.; Wang, J.-J. Aryl  $\lambda^3$ -Iodane-Mediated 6-exo-trig Cyclization to Synthesize Highly Substituted Chiral Morpholines. *Adv. Synth. Catal.* **2015**, *357*, 2788–2794. (b) Li, X.; Li, C.; Zhang, W.; Lu, X.; Han, S.; Hong, R. Highly Stereoselective 7-Endo-Trig/Ring Contraction Cascade To Construct Pyrrolo[1,2-a]quinoline Derivatives. *Org. Lett.* **2009**, *11*, 4036–4039.

(30) Poddel'sky, A. I.; Cherkasov, V. K.; Abakumov, G. A. Transition metal complexes with bulky 4,6-di-tert-butyl-N-aryl(alkyl)-o-imino-benzoquinonato ligands: Structure, EPR and magnetism. *Coord. Chem. Rev.* **2009**, *253*, 291–324.

(31) Panja, A.; Mandal, T. K. Synthesis, crystal structure, redox property and theoretical study of pyrrole containing cobalt(III) Schiff base compound. *Indian J. Chem.* **2016**, *55*, 137.